# Preferential nucleation of dislocation loops under stress explained by A15 Frank-Kasper nanophases in aluminum

Thomas Jourdan, Alexandra Goryaeva, Mihai Cosmin Marinica

# Preferential nucleation of dislocation loops under stress explained by A15 Frank-Kasper nano-phases in aluminum

T. Jourdan,* A. M. Goryaeva, and M.-C. Marinica

*Université Paris-Saclay, CEA, Service de recherche en Corrosion et Comportement des Matériaux, SRMP, F-91191 Gif-sur-Yvette, France*

## Abstract

The asymmetric distribution of geometrically equivalent defects is a longstanding problem in materials science. In this study, we investigate the preferential nucleation of interstitial dislocation loops in specific planes in stressed aluminum, commonly observed experimentally, and seek to clarify the underlying mechanism. For this purpose, we consider a structural change in the geometry of defects, specifically the transformation of 3D compact A15 clusters into 2D Frank loops. Using object kinetic Monte Carlo and *ab initio* calculations, we show that a symmetry breaking in the transformation of A15 clusters significantly impacts the dislocation loop distributions, resulting in the emergence of a preferential orientation when the material is under stress. This discovery not only calls for a critical revision of established theories but also has tangible applications for materials under extreme conditions.


Secondary phase precipitates and self-defect clusters are known to profoundly affect material properties. In many materials, these defects have an anisotropic shape and exhibit several variants, which form evenly if the matrix is isotropic. If a stress is applied, some variants may form preferentially [1, 2]. This asymmetric distribution of defects provides interesting properties to functional materials [3–6], but can also be a source of undesired deformation for structural materials [7]. Although the driving force for preferential formation of variants, namely the minimization of elastic energy, is often invoked, the fundamental mechanisms explaining this phenomenon are still unclear. In particular, kinetic aspects may be crucial in the selection of atomic processes leading to anisotropic microstructures [8].

Here we focus on the phenomenon of interstitial dislocation loop alignment under stress and irradiation, which has been widely reported in the literature [9–15]. This anisotropic formation of loops has been shown to give substantial deformation [16–18] and may explain, at least partially, the primary stage of irradiation creep [7, 19, 20]. It also contributes to anisotropic deformation of thin films irradiated with ions, a phenomenon sometimes called "anisotropic swelling" [21, 22]. Over the last 60 years three main theories have been put forward to explain the alignment of dislocation loops, but none of them appears satisfactory. The first one, known as *stress induced preferred nucleation* (SIPN) [10, 23], relies on the classical nucleation theory for dislocation loops [24] and leads to loop densities proportional to Boltzmann factors depending on the normal stress on the loop planes. However it was shown that owing to the high stability of small interstitial clusters, nucleation of loops does

not occur through a classical nucleation mechanism, at least at moderate temperatures [25]. This flaw in the SIPN model led to the development of another model, based on the reorientation without migration of small interstitial clusters under stress [26, 27]. Although little is known about the dynamics of interstitial clusters under stress, anelastic measurements in aluminum have indeed shown that small clusters may reorient [28]. A tri-interstitial configuration was proposed as the candidate for this reorientation, but the small energy difference between the tri-interstitial configurations under applied stress would induce only a weak loop alignment, inconsistent with experimental results [26]. Finally, a model of differential loop growth under stress, known as *stress induced preferred absorption* (SIPA), has been proposed to explain anisotropy of loop distributions [29]. In this model, favorably oriented loop variants would grow, while the others would shrink and eventually disappear. However, object kinetic Monte Carlo (OKMC) simulations could not confirm any appreciable effect of SIPA on loop behavior [30].

Recently, a new mechanism of loop formation has been evidenced in fcc metals, relying on 3D interstitial clusters with A15 Frank-Kasper phase structure [31]. Although these clusters are metastable in aluminum, they easily form by the successive agglomeration of $\langle 100 \rangle$ dumbbells, prior to the formation of dislocation loops. The complex interaction between kinetic and entropic effects seems to drive the formation mechanism of these compact clusters. Yet, it is unequivocally established that A15 clusters grow under irradiation and, when they reach a critical size, transform into $\frac{1}{3}\langle 111 \rangle$ Frank loops. In aluminum, this transformation occurs when A15 clusters contain 7 self-interstitial atoms (SIAs), through a $\langle 111 \rangle$ screw mechanism involving the collective rearrangement of a few tens of atoms (see Fig. 1 and Ref. [31]). In the present letter, we investigate the role of this transformation mechanism in the loop alignment under stress. By combining Density Functional Theory (DFT) and OKMC calculations, we show that the transformation of A15 clusters into $\frac{1}{3}\langle 111 \rangle$ loops under stress provides an explanation for the experimentally observed anisotropic loop distributions.

Previous OKMC simulations of dislocation loop growth under stress and electron irradiation [30] do not deal with loop nucleation mechanisms in depth. In this study, we introduce A15 clusters and their possible transformation into loops in the OKMC model, with relevant parameters obtained from DFT calculations performed with the VASP code [32, 33]. The full parameterization of OKMC simulations and the DFT simulation setup are provided in the Supplemental Material [34]. We only give here salient features of the model related to

A15 clusters.

The elastic stress field generated by A15 clusters leads to the preferential absorption of SIAs and to the growth of these clusters. A15 clusters can be seen as inhomogeneous Eshelby inclusions [35], which generate a strain field with only a dipole component (in $1/r^3$) when they are spherical. DFT values of elastic dipole tensors of A15 clusters from $I_2^{\mathrm{A15}}$ to $I_7^{\mathrm{A15}}$, obtained with the stress method [36], are given in Table I. Although only $I_7^{\mathrm{A15}}$ is perfectly isotropic, other clusters have nearly isotropic dipole tensors. Therefore we consider them as spherical from an elastic point of view and we use the strain field generated by an isotropic elastic dipole.

TABLE I. Elastic dipole tensor of various cluster configurations

| Configuration | Elastic dipole (eV) | Configuration | Elastic dipole (eV) |
|---|---|---|---|
| $I_2^{\mathrm{A15}}$ | $\begin{bmatrix} 35.02 & 0 & -3.56 \\ 0 & 32.22 & 0 \\ -3.56 & 0 & 33.67 \end{bmatrix}$ | $I_6^{\mathrm{A15}}$ | $\begin{bmatrix} 84.62 & 0. & 0. \\ 0. & 81.92 & 0. \\ 0. & 0. & 84.85 \end{bmatrix}$ |
| $I_3^{\mathrm{A15}}$ | $\begin{bmatrix} 47.52 & 0 & 0.37 \\ 0 & 47.63 & 0 \\ 0.37 & 0 & 48.90 \end{bmatrix}$ | $I_7^{\mathrm{A15}}$ | $\begin{bmatrix} 93.51 & 0. & 0. \\ 0. & 93.51 & 0. \\ 0. & 0. & 93.51 \end{bmatrix}$ |
| $I_4^{\mathrm{A15}}$ | $\begin{bmatrix} 60.25 & 0.33 & -0.33 \\ 0.33 & 60.25 & -0.33 \\ -0.33 & -0.33 & 60.25 \end{bmatrix}$ | $I_7^{\langle 111\rangle}$ | $\begin{bmatrix} 98.88 & 22.22 & 22.22 \\ 22.22 & 98.88 & 22.22 \\ 22.22 & 22.22 & 98.88 \end{bmatrix}$ |
| $I_5^{\mathrm{A15}}$ | $\begin{bmatrix} 70.23 & -2.06 & 0. \\ -2.06 & 73.13 & 0. \\ 0. & 0. & 74.36 \end{bmatrix}$ | $I_7^{\mathrm{A15}} \leftrightarrow I_7^{\langle 111\rangle}$ (saddle point) | $\begin{bmatrix} 97.97 & 7.40 & 7.40 \\ 7.40 & 97.97 & 7.40 \\ 7.40 & 7.40 & 97.97 \end{bmatrix}$ |

The transformation barrier $I_7^{\mathrm{A15}} \rightarrow I_7^{\langle 111\rangle}$, calculated with the climbing image nudged elastic band (CI-NEB) using 7 images, is shown in Fig. 1-a. The starting configuration was the path calculated with an EAM potential in Ref. [31], which was itself found from a systematic exploration of the energy landscape with the Activation-Relaxation Technique nouveau (ARTn) method [38]. Although DFT and EAM paths are virtually the same,

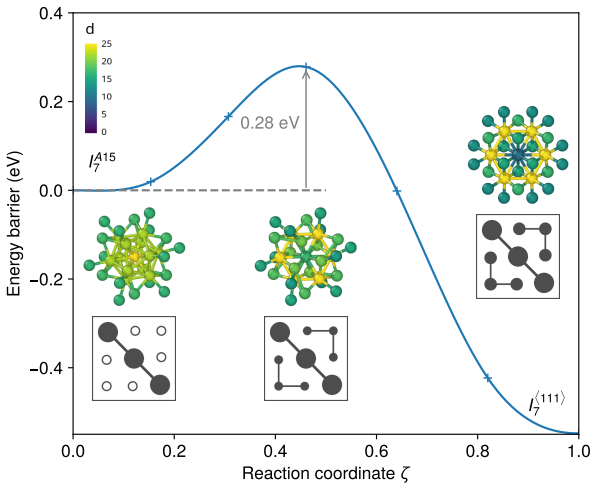


FIG. 1. Energy barrier of the $I_7^{\mathrm{A15}} \rightarrow I_7^{\langle 111\rangle}$ transformation. Atomic structures of defect clusters along the transition path are also shown. Atoms are colored according to the magnitude of the distortion score $d$ [37]. Structures are viewed along the $\langle 111\rangle$ axis. The symmetry of the associated elastic dipole tensor $P_{ij}$ is schematically represented under each configuration. The size of black circles is proportional to the magnitude of components, and equal components are connected with each other. Empty circles refer to components equal to zero. Values of non-zero components are given in Table I.

they differ in two respects: the relative stabilities of the initial and final states are reversed, namely $I_7^{\langle 111\rangle}$ is lower in energy than $I_7^{\mathrm{A15}}$ by 0.55 eV; the transformation barrier from DFT is almost twice as low as that from EAM (0.28 eV vs 0.53 eV). Based on our DFT simulations, we expect that the forward transformation $I_7^{\mathrm{A15}} \rightarrow I_7^{\langle 111\rangle}$ occurs easily at room temperature, whereas the reverse transition should be much less frequent.

In the OKMC simulations, we assume that all SIAs first agglomerate as A15 clusters, as suggested in Ref. [31]. These clusters grow or shrink depending on the type of point defects absorbed. Once an A15 cluster has 7 SIAs, it may also transform into one of the four $\langle 111\rangle$ loop variants (Fig. 2a). Transformation events are handled as other KMC events, so their probability of being selected depends on the transformation rates. For a transformation of $X$ into $Y$, the transformation rate reads (summation over repeated indices is implied)

$$\Gamma_{I_7^X \rightarrow I_7^Y} = \Gamma_0 \exp\left(-\frac{E^{X\rightarrow Y} - \varepsilon_{ij}(P_{ij}^{X\leftrightarrow Y} - P_{ij}^{X})}{k_{\mathrm{B}}T}\right), \tag{1}$$

where $\Gamma_0$ is an attempt frequency, set to $10^{13}$ Hz, $\varepsilon_{ij}$ is the local strain field (sum of the

applied strain and the strain due to other defects in the simulation box), $E^{X\to Y}$ is the transformation barrier without any effect of stress, as shown in Fig. 1, $P_{ij}^{X}$ and $P_{ij}^{X\leftrightarrow Y}$ are the elastic dipoles of configuration $X$ and saddle configuration $X \leftrightarrow Y$, respectively.

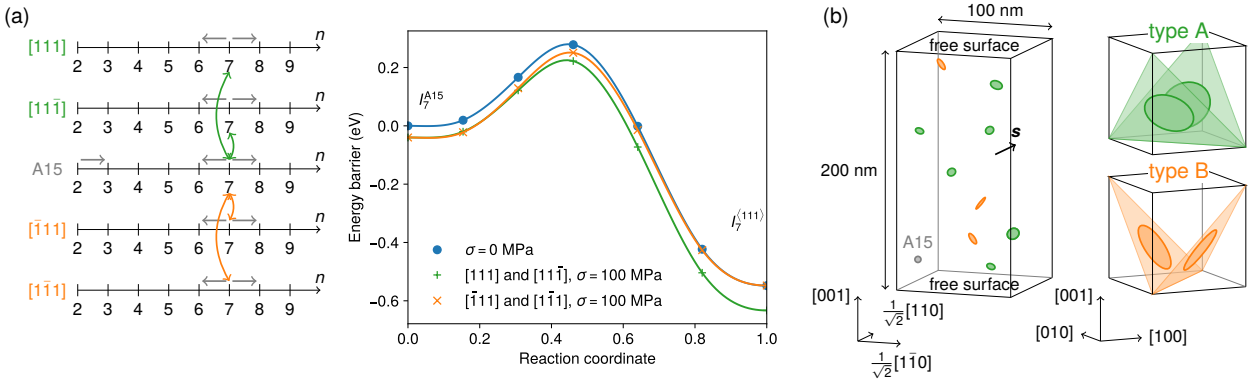


FIG. 2. Schematic representation of OKMC simulations. (a) SIA clusters and transitions between these clusters considered in the present work. $n$ is the number of SIAs in clusters. Five populations are considered: A15 clusters and the four variants of Frank loops. Some transitions are represented with gray, green and orange arrows. SIAs agglomerate as $I_2^{\mathrm{A15}}$ clusters and transitions to and from $\langle 111\rangle$ loops are only possible for $n = 7$. The associated energy barrier under stress ($\sigma = 100$ MPa) is shown for the different variants on the right. (b) Simulation box containing A15 clusters and $\langle 111\rangle$ loops. The direction of applied stress is $\boldsymbol{s}$, so the stress tensor is $\sigma_{ij} = \sigma s_i s_j$. The orientation of $\{111\}$ planes and associated loops with respect to the box axes is schematically represented on the right.

Figure 2b schematically depicts the simulation box used in OKMC simulations. Periodic boundary conditions are imposed along $[1\bar{1}0]$ and $[110]$, whereas free surfaces are used along $[001]$. A stress of magnitude $\sigma = 100$ MPa is applied along $[110]$ and the defect generation rate is 5 $10^{-5}$ dpa/s. This simulation setup aims to be representative of electron irradiations described in Ref. [30], performed on an aluminum thin foil. For the considered stress orientations, the two loop variants $[111]$ and $[11\bar{1}]$ (denoted as "type A" and shown in green in Fig. 2b) are lower in energy by 0.085 eV than $[\bar{1}11]$ and $[1\bar{1}1]$ loops ("type B" loops, shown in orange). Likewise, the energy barrier from $I_7^{\mathrm{A15}}$ to $I_7^{\langle 111\rangle}$ is lower by 0.028 eV for a transition to the two low energy variants (Fig. 2a).

Cluster distributions obtained from 500 simulations are presented in Fig. 3, from 0.1 s to 100 s of irradiation time. Clearly, A15 clusters appear and grow at very short times

($t \leq 0.1$ s), owing to the high diffusion coefficient of SIAs. At these times, A15 clusters already transform into $\langle 111 \rangle$ loops. The transformation of $I_7^{\mathrm{A15}}$ into loops is so fast (the transformation frequency is around $10^9$ Hz) that the concentrations of $I_7^{\mathrm{A15}}$ and larger clusters are negligible. This absence of large A15 clusters is at variance with Frenkel pair accumulation (FPA) simulations performed with an EAM potential [31]: the larger transformation barrier of $I_7^{\mathrm{A15}}$ (0.53 eV, corresponding to a transformation frequency of around $5\ 10^4$ Hz), together with a much larger irradiation flux, may explain this difference. After 1 s of irradiation, the transformation process of A15 clusters is nearly over. The concentrations of type A and type B loops are clearly different (Fig. 3b,c).

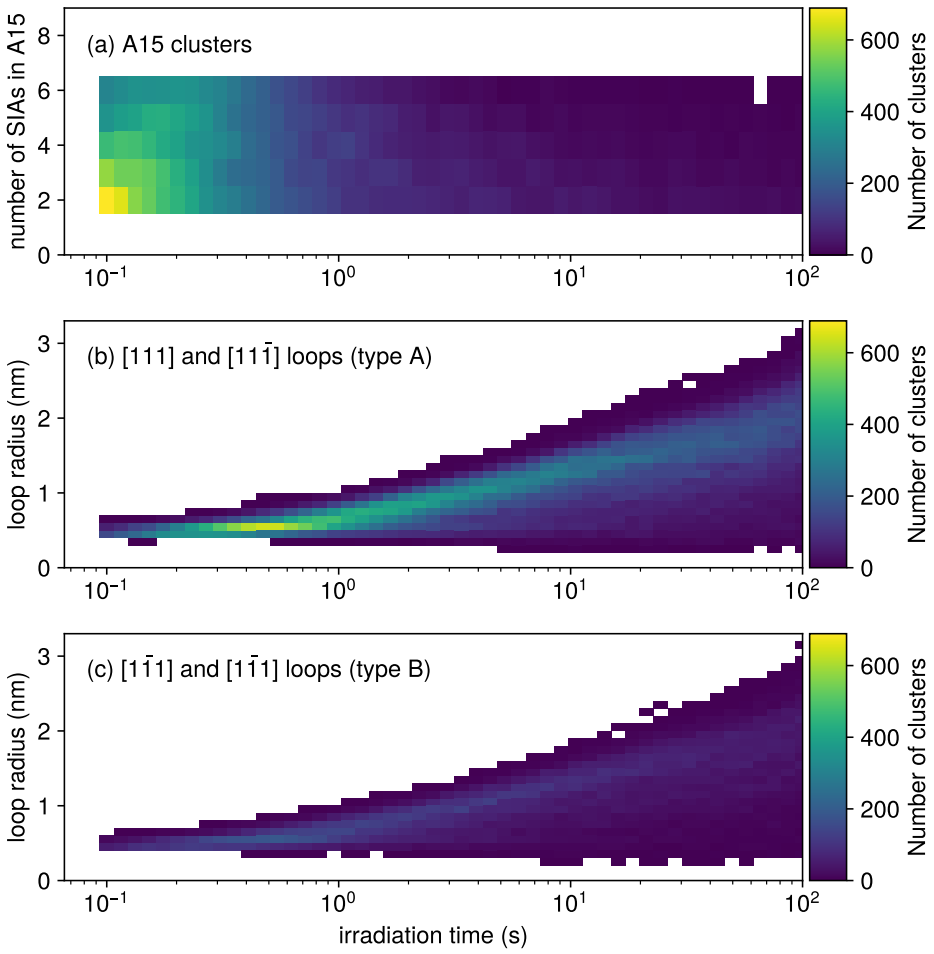


FIG. 3. Particle size distributions for A15 and $\langle 111 \rangle$ clusters as a function of time, calculated over 500 simulations. (a) A15 clusters (b) [111] and [11$\bar{1}$] loops (c) [$\bar{1}$11] and [1$\bar{1}$1] loops. For loops, the radius is represented instead of the number of SIAs in the loops.

To provide a more quantitative insight into the loop alignment process, we represent the proportions of the various clusters in Fig. 4. After a short transient corresponding to the formation of A15 clusters and their transformation into ⟨111⟩ loops, the proportion of clusters remains nearly constant over time, with about 77 % of type A loops and 23% of type B loops. This large imbalance is not so far from the experimental one [30]: type A and type B loops account for 90% and 10% of the loops, respectively. It is also significantly larger than the values obtained with FPA simulations, namely 65.7 % of type A loops and 34.3% of type B loops.

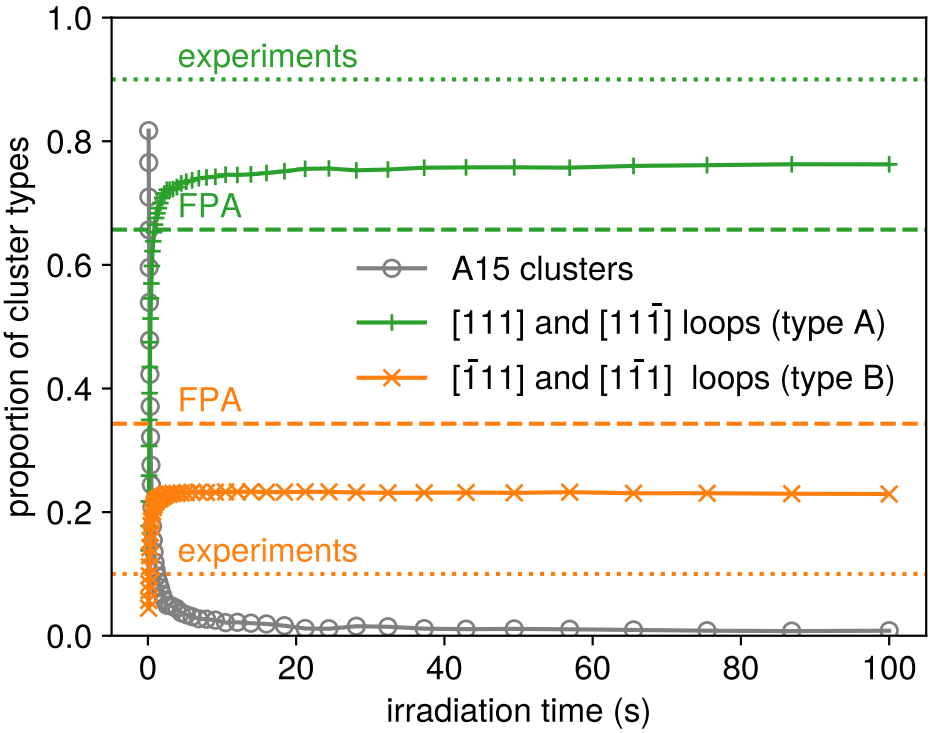


FIG. 4. Proportions of A15 and ⟨111⟩ loops as a function of time. Experimental results at 0.11 dpa are represented by dotted lines and FPA results at 0.03 dpa are represented by dashed lines [30].

As a first approach, one may explain the loop alignment by the different transition rates of $I_7^{\mathrm{A15}}$ to type A and type B loops. From Eq. 1, it can be shown that for a uniaxial stress of magnitude $\sigma$ applied along [110], the ratio of transition rates is simply

$$\frac{\Gamma_{I_7^{A15}\rightarrow I_7^{[111],[11\bar{1}]}}}{\Gamma_{I_7^{A15}\rightarrow I_7^{[\bar{1}11],[1\bar{1}1]}}} = \exp\left(\frac{P\sigma}{\mu k_{\mathrm{B}} T}\right), \tag{2}$$

where $\mu$ is the shear modulus of Al ($\mu$ = 26 GPa) and $P$ is the off-diagonal component of the dipole tensor at *saddle* position, expressed in the crystal basis ($P$ = 7.40 eV). We obtain that there should be around 3 times as many type A loops as type B loops, *i.e.* loop proportions of 75%/25%. These values are close but not equal to those obtained in OKMC simulations.

Actually some reverse transitions $I_7^{\langle 111\rangle} \rightarrow I_7^{A15}$ may also occur. Such events are rare for two reasons: the energy barrier is large, and once a $I_7^{\langle 111\rangle}$ grows by absorption of SIAs, its transformation into an A15 cluster becomes impossible in our model. If we assume that $I_7^{\langle 111\rangle}$ clusters do not grow over the average time required for a transformation into an A15 cluster, an equilibrium between $I_7^{\langle 111\rangle}$ and $I_7^{A15}$ populations is established. The ratio of loop concentrations is then given by Eq. 2, where $P$ now refers to the off-diagonal component of the dipole tensor at *stable* position ($P$ = 22.22 eV). This leads to a proportion of type A and type B loops equal to 96% and 4%, respectively. In practice, equilibrium between loop variants could only be obtained in a very low irradiation flux experiment, where loop growth is extremely slow. Indeed, additional calculations with a flux ten times lower lead to 84 % type A loops and 16% type B loops at the same irradiation dose. Even with the high irradiation flux considered here, we observe that not all loops grow in our simulations (Fig. 3) and a few reverse transformations $I_7^{\langle 111\rangle} \rightarrow I_7^{A15}$ occur, leading to the increase of loop alignment (77%/23%) with respect to the rough estimate based on saddle point considerations (75%/25%). Indeed individual loop growth speeds depend not only on the irradiation flux, but also on the local neighborhood of loops through the overlapping of diffusion fields, which are affected by elastic fields produced by A15 clusters and loops. OKMC inherently includes these aspects and thus provides a convenient way to predict loop proportions, beyond simple approximations such as Eq. (2).

In many experiments, the loop proportion of a given variant was shown to increase with the normal stress on the loop plane $\sigma_{\mathrm{n}} = \sigma_{ij} n_i n_j$, where $\boldsymbol{n}$ is the normal vector [10–13, 15, 30]. This correlation gave support to the SIPN model, which postulates that the loop density should be correlated to the interaction energy of a loop at critical size [39, 40]

$$E = -P_{ij}\varepsilon_{ij} = C_{ijkl} S_k b_l \varepsilon_{ij}, \tag{3}$$

where $C_{ijkl}$ are the elastic constants, $\boldsymbol{S} = S\boldsymbol{n}$ is the surface vector and $\boldsymbol{b}$ is the Burgers vector ($\boldsymbol{b} = -b\boldsymbol{n}$ for a pure prismatic interstitial loop). This energy can be simply rewritten

as [41]

$$E = \sigma_{kl} S_k b_l = -\sigma_{\mathrm{n}} S b. \tag{4}$$

Our OKMC results, performed with a specific stress orientation, agree with the experimental trend, without requiring any SIPN argument. We have shown that when loops are produced by transformation of A15 clusters, key quantities to explain the anisotropic distribution of loops are interaction energies at saddle positions, not stable positions. But since dipole tensors of saddle configurations are similar to those of loops to which they are related (see Fig. 1 and Table I), the present model is expected to behave similary to SIPN and give larger densities for loops with larger normal stresses. This is exactly the case in the framework of isotropic elasticity: for both $\langle 111 \rangle$ stable and saddle configurations, dipole tensors can be written as $P_{ij} = P_0 \delta_{ij} + 3P_1 n_i n_j$, and the only difference in interaction energy between variants is contained in the term $-3P_1 n_i n_j \varepsilon_{ij}$, or equivalently $-3P_1 n_j n_j \sigma_{ij}/2\mu = -3P_1 \sigma_{\mathrm{n}}/2\mu$.

Our simulations unambiguously demonstrate that accounting for the transformation of A15 clusters into $\langle 111 \rangle$ loops results in a remarkable loop alignment under stress, and explains experimental observations. In the experimental conditions investigated in this work, loop alignment is ascribed mostly to the unequivalent forward transitions from A15 clusters into $\langle 111 \rangle$ loops, so it depends mostly on the elastic properties of the saddle configuration. Other mechanisms may be active, especially in other fcc metals where the transition between A15 clusters and loops is more complex [31], so generalizing our result would require further study.

This study provides perspectives on other crystal structures where 3D clusters have been identified as precursors of dislocation loops and loop alignment has been observed. This is the case, for example of iron with compact C15 Laves phase clusters [15, 42–44] and silicon carbide [45, 46]. More generally, it highlights the importance of kinetic barriers on the formation of non equivalent variants of clusters under applied stress. The methodology developed in this work, which achieves atomic resolution in the description of elementary processes while taking account of collective effects on experimental spatial and temporal scales, could be useful for other kinds of systems.

**ACKNOWLEDGEMENTS**

This work has been carried out partly within the framework of the EUROfusion Consortium, funded by the European Union via the Euratom Research and Training Programme (EUROfusion Grant No. 101052200). The views and opinions expressed herein do not necessarily reflect those of the European Commission. AMG, MCM and TJ acknowledge the support from GENCI - (Jean-Zay/CINES/CCRT) computer centre under Grants A0150906973 and A0100912414. TJ gratefully acknowledges Dr. A. Chartier for discussions about A15 clusters observed in FPA simulations.

---

* thomas.jourdan@cea.fr

[1] T. Eto, A. Sato, T. Mori, Stress-oriented precipitation of G.P. zones and $\theta'$ in an Al-Cu alloy, Acta Metall. 26 (1978) 499.

[2] J. Michutta, C. Somsen, A. Yawny, A. Dlouhy, G. Eggeler, Elementary martensitic transformation processes in Ni-rich NiTi single crystals with $Ni_4Ti_3$ precipitates, Acta Mater. 54 (2006) 3525.

[3] D. Y. Li, L. Q. Chen, Selective variant growth of coherent $Ti_{11}Ni_{14}$ precipitate in a TiNi alloy under applied stresses, Acta Mater. 45 (1997) 471.

[4] M. Nastasi, T. Höchbauer, J.-K. Lee, A. Misra, J. P. Hirth, M. Ridgway, T. Lafford, Nucleation and growth of platelets in hydrogen-ion-implanted silicon, Appl. Phys. Lett. 86 (2005) 154102.

[5] A. Radi, J. Khalil-Allafi, M. R. Etminanfar, S. Pourbabak, D. Schryvers, B. Amin-Ahmadi, Influence of stress aging process on variants of nano-$Ni_4Ti_3$ precipitates and martensitic transformation temperatures in NiTi shape memory alloy, Materials and Design 142 (2018) 93.

[6] J. Han, H. Wang, A. Xu, K. Niu, W. Zheng, Externally-Physical-Field-Assisted Aging Precipitation in Aerospace Aluminum Alloys: A Review, Crit. Rev. Solid State 48 (2023) 535.

[7] F. Onimus, T. Jourdan, C. Xu, A. A. Campbell, M. Griffiths, 1.10 - Irradiation creep in materials, in: Comprehensive Nuclear Materials, Elsevier, 2020, p. 310.

[8] F. A. Reboredo, M. Ferconi, S. T. Pantelides, Theory of the nucleation, growth, and structure of hydrogen-induced extended defects in silicon, Phys. Rev. Lett. 82 (1999) 4870.

[9] P. R. Okamoto, S. D. Harkness, Stress-biased loop nucleation in irradiated type 316 stainless steels, J. Nucl. Mater. 48 (1973) 204.

[10] H. R. Brager, F. A. Garner, G. L. Guthrie, The effect of stress on the microstructure of neutron irradiated type 316 stainless steels, J. Nucl. Mater. 66 (1977) 301–321.

[11] D. Caillard, J. L. Martin, B. Jouffrey, Creep under irradiation of 316 steel in the high voltage electron microscope, Acta Metall. 28 (1980) 1059.

[12] T. Atkins, R. J. McElroy, The effects of applied stress on the irradiation induced microstructures of dilute nickel alloys, in: American Society for Testing, Materials (Eds.), Radiation-Induced Changes in Microstructure: 13th International Symposium (Part I), ASTM STP 955, 1987, p. 447.

[13] M. Suzuki, A. Sato, Stress-assisted nucleation of interstitial loops in an electron-irradiated Fe-18Cr-14Ni alloy, J. Nucl. Mater. 172 (1990) 97.

[14] Y. Katoh, S. Kondo, L. L. Snead, Microstructures of beta-silicon carbide after irradiation creep deformation at elevated temperatures, J. Nucl. Mater. 382 (2008) 170.

[15] C. Xu, G. S. Was, Anisotropic dislocation loop distribution in alloy T91 during irradiation creep, J. Nucl. Mater. 454 (2014) 255.

[16] W. G. Wolfer, J. P. Foster, F. A. Garner, The interrelationship between swelling and irradiation creep, Nucl. Technol. 16 (1972) 55.

[17] A. D. Brailsford, R. Bullough, Irradiation creep due to growth of interstitial loops, Philos. Mag. 27 (1973) 49.

[18] K. Herschbach, W. Schneider, Interconnection between irradiation creep and interstitial loop formation in fcc metals, J. Nucl. Mater. 51 (1974) 215.

[19] J. R. Matthews, M. W. Finnis, Irradiation creep models – An overview, J. Nucl. Mater. 159 (1988) 257.

[20] Q. Yu, G. Po, J. Marian, Physics-based model of irradiation creep for ferritic materials under fusion energy operation conditions, J. Appl. Phys. 132 (2022) 225101.

[21] S. Yang, Y. Nakagawa, M. Kondo, T. Shibayama, Anisotropic defect distribution in $He^+$-irradiated 4H-SiC: Effect of stress on defect distribution, Acta Mater. 211 (2021) 116845.

[22] D. R. Mason, S. Das, P. M. Derlet, S. L. Dudarev, A. J. London, H. Yu, N. W. Phillips, D. Yang, K. Mizohata, R. Xu, F. Hofmann, Observation of transient and asymptotic driven structural states of tungsten exposed to radiation, Phys. Rev. Lett. 125 (2020) 225503.

[23] R. V. Hesketh, A possible mechanism of irradiation creep and its reference to uranium, Philos. Mag. 7 (1962) 1417.

[24] K. C. Russel, R. W. Powell, Dislocation loop nucleation in irradiated metals, Acta Metall. 21 (1973) 187.

[25] F. A. Garner, W. G. Wolfer, H. R. Brager, A reassessment of the role of stress in development of radiation-induced microstructure, in: J. A. Sprague, D. Kramer (Eds.), Effects of radiation on structural materials, ASTM STP 683, 1979, p. 160.

[26] W. G. Wolfer, Correlation of radiation creep theory with experimental evidence, J. Nucl. Mater. 90 (1980) 175.

[27] J. Leteurtre, J. L. Pouchou, L. Zuppiroli, Méthode expérimentale d'étude du germe de boucle de dislocation : détermination de sa taille, Philos. Mag. 27 (1973) 1323.

[28] K.-H. Robrock, L. E. Rehn, V. Spirić, W. Schilling, Anelastic relaxation due to clustered self-interstitial atoms in Al, Phys. Rev. B 15 (1977) 680.

[29] W. G. Wolfer, L. K. Mansur, J. A. Sprague, Theory of swelling and irradiation creep, in: M. L. Bleiberg, J. W. Bennett (Eds.), Radiation Effects in Breeder Reactor Structural Materials, The Metallurgical Society of AIME, 1977, p. 841.

[30] D. Da Fonseca, F. Mompiou, T. Jourdan, J.-P. Crocombette, A. Chartier, F. Onimus, Evidence of dislocation loop preferential nucleation in irradiated aluminum under stress, Scr. Mater. 233 (2023) 115510.

[31] A. M. Goryaeva, C. Domain, A. Chartier, A. Dézaphie, T. D. Swinburne, K. Ma, M. Loyer-Prost, J. Creuze, M.-C. Marinica, Compact A15 Frank-Kasper nano-phases at the origin of dislocation loops in face-centred cubic metals, Nat. Commun. 14 (2023) 3003.

[32] G. Kresse, J. Furthmüller, Efficient iterative schemes for *ab initio* total-energy calculations using a plane-wave basis set, Phys. Rev. B 54 (1996) 11169.

[33] G. Kresse, J. Furthmüller, Efficiency of ab-initio total energy calculations for metals and semiconductors using a plane-wave basis set, Comput. Mater. Sci. 6 (1996) 15.

[34] See Supplemental Material at [url], which includes Refs. [47–55], for additional information about the parametrization of OKMC simulations and the DFT simulation setup.

[35] J. D. Eshelby, The determination of the elastic field of an ellipsoidal inclusion, and related problems, Proceedings of the Royal Society of London. Series A. Mathematical and Physical Sciences 241 (1957) 376.

[36] C. Varvenne, E. Clouet, Elastic dipoles of point defects from atomistic simulations, Phys. Rev. B 96 (2017) 224103.

[37] A. M. Goryaeva, C. Lapointe, C. Dai, J. Dérès, J.-B. Maillet, M.-C. Marinica, Reinforcing materials modelling by encoding the structures of defects in crystalline solids into distortion scores, Nat. Commun. 11 (2020) 4691.

[38] N. Mousseau, L. K. Béland, P. Brommer, J.-F. Joly, F. El-Mellouhi, E. Machado-Charry, M.-C. Marinica, P. Pochet, The Activation-Relaxation Technique: ART Nouveau and Kinetic ART, J. Mol. Opt. Phys. 2012 (2012) 1.

[39] E. Clouet, C. Varvenne, T. Jourdan, Elastic modeling of point-defects and their interactions, Comp. Mater. Sci. 147 (2018) 49.

[40] S. L. Dudarev, P.-W. Ma, Elastic fields, dipole tensors, and interaction between self-interstitial atom defects in bcc transition metals, Phys. Rev. Mater. 2 (2018) 033602.

[41] W. G. Wolfer, T. Okita, D. M. Barnett, Motion and Rotation of Small Glissile Dislocation Loops in Stress Fields, Phys. Rev. Lett. 92 (2004) 085507.

[42] M.-C. Marinica, F. Willaime, J.-P. Crocombette, Irradiation-induced formation of nanocystallites with C15 Laves phase structure in bcc iron, Phys. Rev. Lett. 108 (2012) 025501.

[43] A. Chartier, M.-C. Marinica, Rearrangement of interstitial defects in alpha-Fe under extreme condition, Acta Mater. 180 (2019) 141.

[44] J. Gao, E. Gaganidze, J. Akta, Relative population of $1/2\langle 111\rangle$ and $\langle 100\rangle$ interstitial loops in alpha-Fe under irradiation: Effects of C15 cluster stability and loop one-dimensional movement, Acta Mater. 233 (2022) 117983.

[45] H. Ko, A. Kaczmarowki, I. Szlufarska, D. Morgan, Optimization of self-interstitial clusters in 3C-SiC with genetic algorithm, J. Nucl. Mater. 492 (2017) 62.

[46] T. Koyanagi, D. J. Sprouster, L. L. Snead, Y. Katoh, X-ray characterization of anisotropic defect formation in SiC under irradiation with applied stress, Scr. Mater. 197 (2021) 113785.

[47] P. E. Blöchl, Projector augmented-wave method, Phys. Rev. B 50 (1994) 17953.

[48] G. Kresse, D. Joubert, From ultrasoft pseudopotentials to the projector augmented-wave method, Phys. Rev. B 59 (1999) 1758.

[49] C. Varvenne, F. Bruneval, M.-C. Marinica, E. Clouet, Point defect modeling in materials: Coupling *ab initio* and elasticity approaches, Phys. Rev. B 88 (2013) 134102.

[50] D. Carpentier, T. Jourdan, Y. Le Bouar, M.-C. Marinica, Effect of saddle point anisotropy of point defects on their absorption by dislocations and cavities, Acta Mater. 136 (2017) 323.

[51] D. Da Fonseca, F. Onimus, F. Mompiou, M.-C. Marinica, E. de Sonis, E. Clouet, T. Jourdan, Numerical investigation of dislocation climb under stress and irradiation, Acta Mater. 242 (2023) 118431.

[52] H. Wang, D. Rodney, D. Xu, R. Yang, P. Veyssière, Pentavacancy as the key nucleus for vacancy clustering in aluminum, Phys. Rev. B 84 (2011) 220103.

[53] D. Connétable, M. David, Study of vacancy-(H,B,C,N,O) clusters in Al using DFT and statistical approaches: Consequences on solubility of solutes, J. Alloys Compd. 748 (2018) 12.

[54] P. Ehrhart, P. Jung, H. Schultz, H. Ullmaier, Landolt–Börnstein, Numerical Data and Functional Relationships in Science and Technology, Atomic Defects In Metals, Springer, 1991.

[55] C. C. Fu, F. Willaime, P. Ordejón, Stability and mobility of mono- and di-interstitials in $\alpha$-Fe, Phys. Rev. Lett. 92 (2004) 175503.